УДК 547.458.8

Mechanical and Permeability Properties of Thermoplastic Starch Composites Reinforced with Cellulose Nanofiber for Packaging Applications

Preetha Balakrishnan[a], Sreerag Gopi[b], V.G. Geethamma[a] and Sabu Thomas*[a,c]

[a]International and Inter University Center for Nanoscience and Nanotechnology, Mahatma Gandhi University Kottayam, Kerala, 686560, India
[b]ADSO Naturals Pvt., Ltd. 2/5 RMV Second Stage, Sanjay Nagar, Bangalore, 560094, India
[c]School of Chemical Sciences, Mahatma Gandhi University Kottayam, Kerala, 686560, India

In this study, a facile, ecofriendly nanocomposite based on glycerol-plasticized thermoplastic potato starch (TPS) containing 0-4 wt.% cellulose nanofiber (CNF) from pineapple leaf was prepared by the solution casting technique. The nanocomposite films showed better mechanical properties compared to neat film. The tensile properties were fit with theoretical predictions. Tensile strength increased with CNF loading and reached up to 4.682 MPa (TPS+3 wt.% CNF) from 1.58 MPa (neat TPS), an improvement of ~196% over the neat polymer. The addition of cellulose nanofiber improved the barrier properties of films by creating a tortuous path for penetrant molecules. Gas transport behavior of CNF-based TPS nanocomposite films was explored using O_2 gas. A 56% decrease (relative to neat TPS) in oxygen permeability of the nanocomposite membranes was achieved by adding only 3 wt.% CNF. The oxygen permeability data were fit with two theoretical models.

Keywords: starch, nanofiber, mechanical, permeability, modeling.

*   Corresponding author E-mail address: sabuchathukulam@yahoo.co.uk
ORCID: 0000-0001-8268-0828 (Balakrishnan P.); 0000-0002-4476-6433 (Gopi S.); 0000-0003-4726-5746 (Thomas S.)

Механические свойства и проницаемость термопластичных крахмальных композитов, армированных нановолокнами целлюлозы, для применения в качестве упаковки

П. Балакришнан[а], С. Гопи[б], В.Г. Геетхамма[а], С. Томас[а,в]

[а]*Международный и межвузовский центр нанонауки и нанотехнологий, Университет Махатмы Ганди Индия, 686560, Керала, Коттаям*
[б]*ООО "ADSO Naturals" Индия, 560094, Бангалор, Санджай Нагар, РМВ Стейдж 2, 2/5*
[в]*Факультет химических наук, Университет Махатмы Ганди Индия, 686560, Керала, Коттаям*

Описан легкий, экологически чистый нанокомпозит на основе пластифицированного глицерином термопластичного картофельного крахмала (ТКК), содержащий 0-4 мас.% целлюлозного нановолокна (ЦН) из листьев ананаса, полученный методом испарения из раствора. Нанокомпозитные пленки имели улучшенные механические свойства по сравнению с исходной пленкой из крахмала. Свойства на растяжение соответствовали теоретическим предсказаниям. Предел прочности на растяжение композитных пленок повышался при увеличении содержания ЦН с 1,58 МПа (чистый ТКК) до 4,682 МПа (ТКК + 3 мас.% ЦН); это улучшение составило ~ 196 % по сравнению с чистым полимером. Добавление целлюлозного нановолокна улучшало барьерные свойства пленок за счет извилистого пути для проникающих молекул. Газотранспортное поведение нанокомпозитных пленок ТКК-ЦН было исследовано с использованием газообразного кислорода. Ведением всего 3 % ЦН было достигнуто 56%-ное уменьшение кислородной газопроницаемости композитных пленок по сравнению с чистым ТКК. Данные по кислородной проницаемости соответствовали двум теоретичеким моделям.

Ключевые слова: крахмал, нановолокно, механические свойства, проницаемость, моделирование.

Introduction

Biopolymers from renewable resources have recently attracted considerable attention because of their unique properties, including ease in fabrication, low cost and biodegradability (Guohua et al., 2006; Tang and Alavi, 2011). Renewable polymers offer an attractive alternative to maintain sustainable development and an ecofriendly nature (Halley, 2005). The biodegradable nature of these materials will lead to a reduction in carbon dioxide concentration in the environment and they may even replace many synthetic polymers. In recent years, petroleum-based packaging materials lost attention because of increasing environmental pollution. In this scenario, biopolymer composites gain

importance. In the family of renewable polymers, starch has been considered to be one of the most promising materials because of its availability, cost effectiveness, and biodegradability.

Starch is a semicrystalline polymer composed of two polysaccharides: amylose, a linear molecule, and highly branched amylopectin. The proportion of amylose and amylopectin varies from plant to plant. Nevertheless, without plasticizers the films made from starch are brittle in nature and not easy to fabricate. Plasticizers are low molecular weight, highly volatile molecules that can enter in between the starch macromolecular chains and thereby reduce the inter- as well as intramolecular interactions in starch (Biduski et al., 2018; Mlalila et al., 2018).

Sustainable food packaging has a substantial impact on quality, taste, and marketability of products. As per the WHO, approximately 40% of all food products spoil every year in the United States (Wang et al., 2018). Limitations in harvesting, transporting and storage all contribute to this spoilage. The quality of packaging that prevents oxygen and water vapor from coming into contact with food is a major cause of food spoilage.

Shelf life plays an important role in determining the quality of film, and it depends mainly on the humidity and gas permeability through the film. A humid atmosphere with the presence of oxygen favors microbial growth and gradually spoils the quality of food inside (Malmir et al., 2017; Nair et al., 2017). Moreover, the reduced transmission rate favors increasing the degradation rate, since it depends on the transport of water from the surface to the bulk of the material (Park et al., 2003). In that respect, the Water Vapor Transmission Rate (WVTR) and Oxygen Transmission Rate (OTR) measurements of representative films were evaluated as the most important parameters for these properties (Wang et al., 2018).

Cellulose is one of the unique biopolymers that can be used to reinforce starch-based films. Cellulose can be extracted from a wide variety of sources, which include hemp (Gironès et al., 2012), wheat straw (Montaño-Leyva et al., 2011), pineapple leaf (Arib et al., 2006), cotton (Prachayawarakorn et al., 2010), bacterial cellulose (Grande et al., 2009), etc. One of the important benefits of using cellulose as a reinforcing phase for starch is its similar polysaccharide structure. Starch, which is a hydrophilic polymer, is incompatible with most synthetic polymers.

Low mechanical properties and barrier properties of biopolymers such as starch have limited their large-scale applicability (Di et al., 2006; Müller et al., 2009). Different methods have been proposed to overcome this limitation including blending (Hoyos et al., 2011), cross-linking (Canisag, 2015), UV irradiation (Narayanan et al., 2017), reinforcing (Balakrishnan et al., 2017), etc. These are all common modification techniques to improve the performance of biopolymer composites.

The aim of this paper is to investigate the effect of the filler aspect ratio on mechanical and barrier properties of the polymer and to quantitatively model the results. Starch nanocomposites containing 0-4 wt.% of cellulose nanofiber were prepared by the solution casting technique. The mechanical properties, water vapor and oxygen permeability, and UV characteristics were investigated. The combined effects of filler concentration and aspect ratio on the barrier properties and mechanical performance of thermoplastic starch (TPS) were investigated, and a tortuous path equation was derived to model the results.

Materials and Methods
Materials

For the fabrication of thermoplastic starch, potato starch (supplied by Lobha chem India

Pvt. Ltd. Mumbai) and glycerol (98% Purity, supplied by Merck India Pvt. Ltd) were used. For nanofiber synthesis, sodium hydroxide, oxalic acid, and hydrogen peroxide were supplied by MERCK India Pvt. Ltd. Cellulose nanofibers were isolated from pineapple leaf with an average diameter of 20-25 nm according to our previous work (Balakrishnan et al., 2017). Briefly, finely chopped pineapple leaves were washed, dried and milled to fine powder. The powder was then subjected to steam explosion using 2% NaOH solution in an autoclave at 138 kPa for 1 hour. Alkali treated fiber was then washed with distilled water until free from alkali, which was confirmed by pH meter measurements. Then, alkali treated fiber was bleached with hydrogen peroxide in an autoclave maintained at 138 kPa. Then, pressure was released abruptly after 30 minutes. This process continued until the residue became white. The bleached fiber was subjected to acid hydrolysis using an 11% oxalic acid solution in an autoclave. Finally, the resultant suspension after acid hydrolysis was centrifuged at 8000 rpm for 6 minutes and dialyzed in tap water for 2 days (Balakrishnan et al., 2017).

Preparation of thermoplastic potato starch (TPS)/cellulose nanofiber (CNF) composites

Thermoplastic starch cellulose nanocomposites were prepared by the solution casting technique. Calculated amounts of cellulose nanofibers were dispersed in distilled water and bath sonicated for 30 minutes. Preweighed potato starch was mixed well with 30% glycerol (on a dry starch basis) using a mechanical stirrer by adding 100 ml distilled water. The suspension of cellulose nanofiber was added to a starch-glycerol water mixture and mixed in a mechanical stirrer (700 rpm) for 30 minutes at a temperature of 90 °C. After the solution became viscous, it was poured on to

leveled borosilicate glass Petri dishes and kept at 50°C for 12 h until it was completely dry. Solution cast films of TPS cellulose nanofiber composites were made at 1, 2, 3, 4 wt.% nanofiber concentrations (as per the dry weight of the matrix). Films of approximately 80 μm thickness were obtained by this technique.

Transmission electron microscopy

The morphology of prepared nanofibers was evaluated using high-resolution transmission electron microscopy (JEM-2100 HRTEM, JEOL, Japan). A drop of well sonicated dilute suspension was drop-cast on a copper grid and dried under an IR lamp.

Mechanical properties

Tensile properties of the films were evaluated by a Smitweld tensile testing unit in accordance with the ASTM 638 Standard. The tensile test was carried out at room temperature with a crosshead speed of 10 mm/min and load cell of 5 kN. Five dumbbell shaped samples of each system were used to determine Young's modulus, tensile strength and elongation at break. The tensile modulus was taken as the slope of the initial linear region of the stress-strain curve.

Water vapor transmission rate

The WVTR of the films was determined according to the ASTM E96-95 Standard (desiccant method). The films were cut into circles with a diameter of 6.3 cm and sealed onto an aluminum permeation cup containing 45 g of dry calcium chloride with silicone grease, and a ring was used to hold the films in place. The whole device was weighed and then placed in a climate-controlled chamber (32°±2°C and 50±5% RH). The permeability cups with the films were weighed at regular time intervals, and a linear relationship was obtained between

the quantity of water transferred per unit of air and time. Water vapor permeability (WVP) for three specimens of each sample was calculated as shown by equation 1:

$$WVTR = \frac{m_2 - m_1}{1440 * r^2} \qquad (1)$$

where m_2 and m_1 are the final and initial weight, respectively, and r is the radius of the permeation cup.

Oxygen transmission rate

The samples were conditioned at a temperature of 23±2°C and 50±5% RH 24 h before measuring the OTR. OTR was determined at the same conditions using a Perme OX2/230 (Labthink Instruments Co., Ltd.). Film thickness was measured with an electronic digital caliper before testing and input to the computer program WinPerme OX2-230 W3-330(En). The OTR was measured after the film had been placed in a cell, and oxygen flow was introduced on one side of the film. The OTR (ml m^{-2} day^{-1}) was calculated from the mean OTR multiplied by the film thickness (mm) and divided by the oxygen gradient within the cell of the testing machine (1 kgf cm^{-2}). Three independent determinations were carried out for each film sample, and the mean of those three values is given as the final result.

UV-Vis spectroscopy

Transparency of the TPS and the TPS-CNF films was studied using UV/Visible light spectroscopy. A Perkin Elmer UV/Vis Spectrometer Lambda 2S (Überlingen, Germany) was used to measure the light transmittance of the films in a light wavelength area from 300 to 1000 nm. The scanning speed used in the analysis was 240 nm/min, and three replicates of each material were measured.

Results and discussion
Morphology of nanofibers

Figure 1 shows the TEM images of cellulose nanofibers. From the image, we notice that the fibers tend to aggregate, which is due to strong inter- and intramolecular interactions between adjacent fibers. The average diameter of fibers was approximately 25 nm, which was calculated by ImageJ software. The length of nanofibers could not be calculated due to the interconnecting structure of fibers. The long fibrous structure facilitates better adhesion of the fibers to the matrix and acts as a barrier against oxygen and water vapor.

Tensile properties

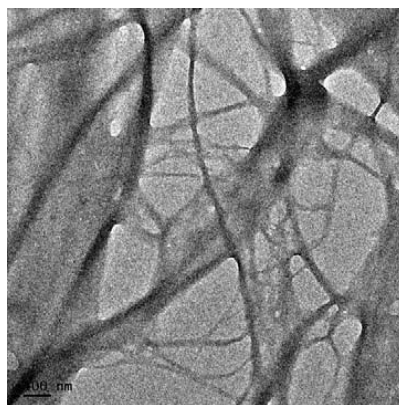Stress-strain behavior characterizes the reinforcing effect of filler onto the matrix. Typical

Fig. 1. TEM image of cellulose nanofiber

stress-strain curves of thermoplastic starch and thermoplastic starch reinforced with CNF isolated from pineapple leaf fiber are shown in Fig. 2. Tensile strength, modulus and elongation increase as filler concentration increases (Table 1). The maximum improvement in tensile strength was observed for 3 wt.% CNF. This is because the thermoplastic starch transmits and distributes stress to the nanofibers, resulting in higher tensile strength of the composites. Thus, the composite can withstand a higher load before failure compared to neat TPS. Figure 2 also shows an incremental increase in moduli (curved slopes) and strength with an increase in the reinforcing phase. The improvement in this mechanical property may be attributed to the following reasons: (1) higher mechanical strength of CNF, (2) better reinforcing efficiency of CNF to the TPS matrix due to the same polysaccharide functionality, and (3) effective dispersion of CNF in the thermoplastic starch (up to 3 wt.% CNF, and beyond that, agglomeration occurs).

Values of tensile strength, percentage of elongation, and tensile modulus of the composite are shown in Table 1. These values were obtained as averages of five measurements per set of composites. Both the tensile strength and modulus increased with increasing nanofiller content. The enhanced mechanical performance of the composites revealed better reinforcing efficiency of cellulose nanofibers to the thermoplastic starch matrix. The tensile strength of neat TPS is 1.58 MPa, reaching
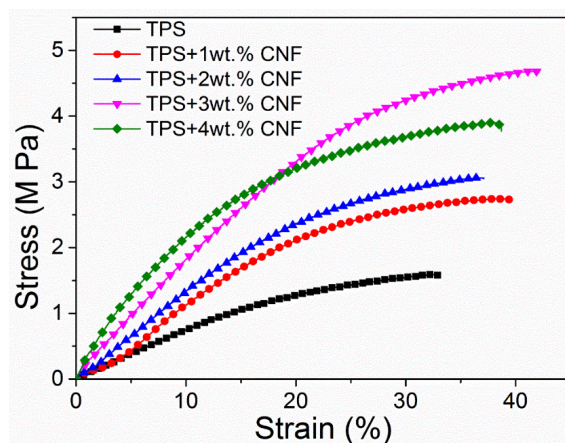

Fig. 2. Stress-Strain curves of TPS-CNF nanocomposites

Table 1. Tensile strength, elongation at break and tensile modulus values of nanocomposites at various filler loadings

Sample	Maximum tensile strength (MPa)	% Elongation	Young's modulus (MPa)
TPS	1.580± 0.11	33.150± 4.6	0.0735± 0.12
TPS+1 wt.%CNF	2.763± 0.25	39.670± 3.8	0.0745± 0.25
TPS+2 wt.%CNF	3.041± 0.15	36.780± 3.9	0.1287± 0.13
TPS+3 wt.%CNF	4.682± 0.31	42.338± 4.9	0.1830± 0.26
TPS+4 wt.%CNF	3.875± 0.14	38.633± 4.8	0.2553± 0.39

a value of 4.68 MPa upon the addition of 3 wt.% nanofiller: an improvement of almost ~198% compared to the virgin polymer. A fine dispersion of cellulose nanofibers over the starch matrix results in an effective load transfer from matrix to filler, which results in uniform stress distribution and minimizes the stress concentrated centers. Another possible reason for the reinforcement is the high surface to volume ratio interacting with the matrix. Upon the addition of filler, the modulus of the composite was also found to increase without reducing the tensile strength, and this dynamic is due to appropriate impregnation of the filler in the matrix and good interfacial adhesion by hydrogen bonding interactions.

Modeling of tensile results

Two of the most widely used models (the Halpin-Tsai Model and Kraus Model) were selected from literature. The main purpose was to predict the modulus of the starch/cellulose system. Typical parameters in such models include the moduli of the matrix and filler, the adhesion between fillers and the host polymer matrix, the volume fraction of the filler and the filler shape factor (e.g., aspect ratio).

Halpin-Tsai Model

To date, many mechanical models have been proposed to explain the mechanical properties of polymer nanocomposites. Among these models, the Halpin-Tsai model is widely used to predict the modulus of fiber-filled nanocomposites as a function of filler content from the moduli of the pure matrix and filler material and the aspect ratio of the filler.

In this study, among all of the models used to predict the elastic modulus of composite materials, the Halpin-Tsai model was used to fit the experimental data. The relative modulus of the composite was evaluated using equation 2.

$$\frac{E_c}{E_m} = \frac{1 + w \frac{\left(E_f/E_m\right) - 1}{\left(E_f/E_m\right) + w} \emptyset}{1 - \frac{\left(E_f/E_m\right) - 1}{\left(E_f/E_m\right) + w} \emptyset} \qquad (2)$$

In this equation, E_c is the modulus of composite, E_m is the modulus of matrix, E_f is the modulus of filler, w is the shape factor 2l/d, ø is the volume fraction of filler, and β is a constant (orientation factor).

In our case, we isolated nanofibers, and the modulus of the filler was calculated using equation 3:

$$E_f = \frac{(w + \emptyset)E_c - w(1 - \emptyset)E_m}{\beta[(w\emptyset + 1)E_m + (1 - \emptyset)E_c]} E_m. \qquad (3)$$

CNF used in this study has an average diameter of approximately 25 nm, as obtained from TEM analysis. The filler volume fraction is a function of the CNF nanofiber weight fraction and the densities of both the filler and matrix. Since the length of nanofiber was not easy to estimate, we took three different lengths including 500 nm, 1 μm, and 2 μm, to calculate the aspect ratio.

Halpin-Tsai equation was originally used for composites with unidirectional reinforcement, but later it was modified and improved to account for the randomness of discontinuous fibers by introducing an orientation factor (β). If the fiber length is greater than the thickness of the specimen, the fibers are assumed to be randomly oriented in two dimensions, and the orientation factor (β) is 1/3. If the fiber length is smaller than the thickness of the specimen, the fibers are assumed to be randomly oriented in three dimensions, and the orientation factor (β) is 1/6. Herein, β is considered to be 1/6, and the Halpin-Tsai equation can be modified to become:

$$\frac{E_c}{E_m} = \frac{1+w\frac{\beta\left(E_f/E_m\right)-1}{\beta E_f/E_m+w}\emptyset}{1-\frac{\beta\left(E_f/E_m\right)-1}{\beta\left(E_f/E_m\right)+w}\emptyset}. \qquad (4)$$

From Fig. 3 we can observe that the model fits well with highest aspect ratio filler. This could be a possible reason for improved performance of composite films.

Kraus Model

The theory was developed by Kraus in 1963 to account for solvent restriction due to fillers in the polymeric network (Kraus, 1963). Due to the enhancement of the polymer-filler interaction, the polymer is reinforced upon the addition of fillers. The reinforcement of the thermoplastic starch matrix can be analyzed from the Kraus plot. Assuming that the filler has completely restricted the swelling of matrix, the following relation is obtained.

$$\frac{V_{ro}}{V_{rf}} = 1 - m\left[\frac{f}{(1-f)}\right], \qquad (5)$$

$$V_{ro} = \frac{d/\rho_p}{d/\rho_p+\left(A_s/\rho_s\right)}, \qquad (6)$$

$$V_{rf} = \frac{\frac{(d-fw)}{\rho_p}}{\left[d-fw/\rho_p\right]+\frac{A_s}{\rho_p}} \qquad (7)$$

where V_{ro} and V_{rf} are volume fractions of solvent swollen matrix in the fully swollen unfilled sample and in the fully swollen filled sample; f is the volume fraction of filler; slope m is the direct measure of the reinforcing capacity of filler in the matrix; d is the weight of the sample without swelling; ρ_p is the density of the polymer; ρs is the density of the solvent; and A_s is the amount of solvent adsorbed by the sample. Vr_0 is a constant for a particular system. Since equation 5 is linear, the plot of $\frac{V_{ro}/V_{rf}}{\frac{f}{(1-f)}}$ gives a straight line with slope m. In Fig. 4, $\frac{V_{ro}}{V_{rf}}$ is plotted against $\frac{f}{(1-f)}$ using water as solvent. It can be seen from the graph that $\frac{V_{ro}}{V_{rf}}$ decreases with CNF loading. According to Kraus theory, a negative slope value indicates a better reinforcement effect. Figure 4 shows a negative slope and, hence, better interaction of CNF in the thermoplastic starch matrix (Kraus, 1963; Abraham et al., 2015).

Water vapor transmission rate (WVTR)

Water vapor permeability results can be useful to understand possible mass transfer
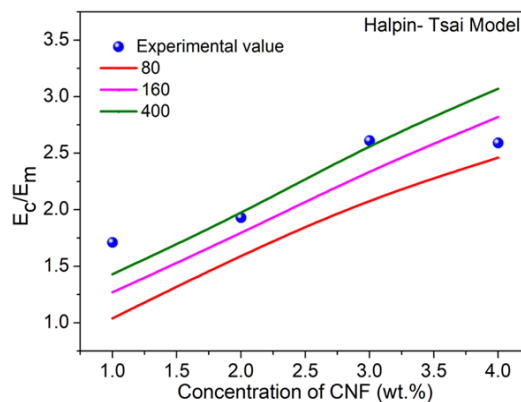

Fig. 3. Theoretical modeling of Young's modulus using different aspect ratios for CNF – comparison with experimental data
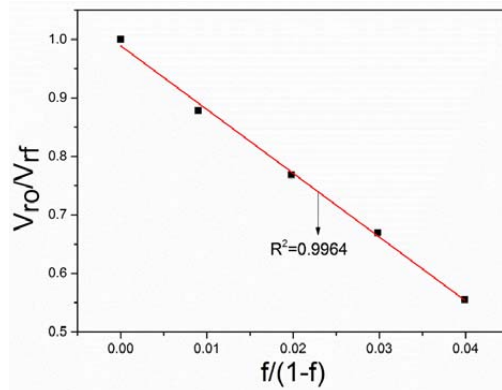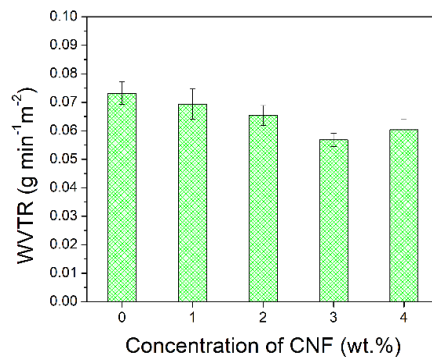
Fig. 4. Kraus plot for TPS/CNF nanocomposites

Fig. 5. WVTR of composite films with varying percentages of cellulose nanofibers

mechanisms and solute and polymer interactions in edible films. According to the thermodynamics of irreversible processes, the water chemical potential difference is the driving force of the water transfer through a film (Chivrac et al., 2010; Tan and Thomas, 2016). When the process occurs at constant temperature and pressure, the water chemical potential difference is proportional to water vapor concentration difference between the two faces (Bertuzzi et al., 2007). The permeability of unmodified thermoplastic film is 0.073 ± 0.004 g min^{-1}m^{-2} (Fig. 5). However, the WVP values decrease after each filler reinforcement, possibly due to their nanoscopic size and better adhesion to the matrix phase and due to the fine dispersion of nanofibers over the starch matrix producing strong hydrogen bonding, which hinders molecules entering into the nanocomposites. Lower WVP was recorded for TPS modified with 3 wt.% CNF 0.0568 ± 0.002 g min^{-1}m^{-2} compared to unmodified starch films. However, at 4 wt.% loading, the permeability increases slightly because of the chance of agglomeration at higher filler loading.

Oxygen permeability

Relative oxygen permeability of nanocomposites with different filler loading is shown in Fig. 6. From the figure, it can be seen that the relative permeability of the composite decreases after each nanofiller inclusion. This finding is consistent with the abovementioned results. The decrease in oxygen permeability can be directly correlated to the filler dispersion and
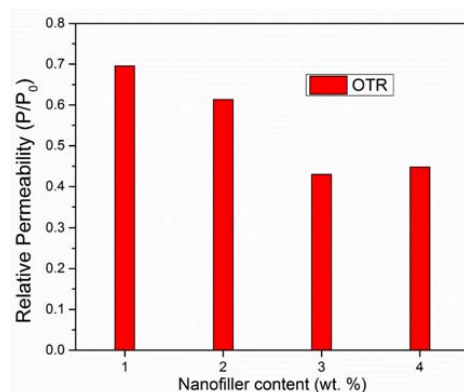
Fig. 6. Oxygen permeability of TPS/CNF nanocomposites

better matrix filler adhesion reducing the free volume within the matrix as well as a decrease in the diffusivity created by the incorporated nanofillers, which creates a tortuous pathway for the penetrant gas molecules. The permeation of gas molecules through a polymeric system is primarily due to two main reasons: diffusivity of the penetrant molecule and penetrant solubility. The drop in these two factors affects the penetration of solvent molecule. Zeppa et al. studied the oxygen barrier properties of potato starch reinforced with closite 30 B, and upon the addition of 6.25 wt.% nanofiller, they reported a relative permeability of 0.87 (Zeppa et al., 2009). Later, Sadegh-Hassani and Mohammadi Nafchi (2014) studied the permeability of potato starch reinforced with Halloysite clay and reported an average permeability of 0.59 upon the addition of 3 wt.% nanoclay. In our present work, with nanofibers isolated form pineapple, we obtained a good permeability resistance as per the earlier reported data. Upon the addition of 3 wt.% CNF, the relative permeability obtained was 0.43, which is lower than the data reported in the literature.

Based on Nielsen's model of tortuosity, it is possible to calculate the permeability reduction achieved by the nanocomposite in the presence of cellulose nanofibers. The reduction in permeability coefficients means that gases should travel in a longer diffusive path. The relationship between tortuosity and permeability as given by Nielsen☐s (Nielsen, 1967) model is

$$\frac{P}{P_o} = \frac{1 - \emptyset_s}{\tau} \tag{8}$$

where P and P_0 are the oxygen permeabilities of the nanocomposite and the matrix without nanofiller, respectively. $\emptyset_s$ is the volume fraction of filler, and τ is tortuosity. The results of the oxygen permeability measurements are summarized in Table 2. Similar findings were reported earlier by Sadegh-Hassani and Mohammadi Nafchi (2014).

Tortuosity created by nanofiber inclusion is primarily due to the fibrous network structure of cellulose nanofibers, which creates less free volume within the matrix and a difficult path for the oxygen molecule to penetrate.

Modeling of permeability mechanism

To predict the permeability of gases through the nanocomposite membrane, several models have been proposed. Relative oxygen permeability of the composite to the neat polymer matrix can be modeled by the geometric path developed by Bharatwaj, which suggests the orientation of impermeable disk plate-like particles dispersed within the matrix.

Table 2. Oxygen permeability values of nanocomposites

Wt.% CNF	Oxygen Permeability $(cm^3\,m^{-2}\,d^{-1})$	Relative permeability (P/P_0)	τ
0	29.440 ± 2.44	1	1
1	20.457 ± 1.37	0.6949	1.42
2	18.005 ± 1.68	0.6116	1.60
3	12.682 ± 2.04	0.4308	2.25
4	13.160 ± 1.54	0.4470	2.15

$$\frac{P}{P_o} = \frac{1-\emptyset_i}{1+\frac{\propto}{2}\emptyset_i\left[\frac{2}{3}\right]\left[O+\frac{1}{2}\right]} \qquad (9)$$

where $\frac{P}{P_o}$ = relative permeability; $\emptyset_i$ = volume fraction of nanofiller; $\propto$ = aspect ratio of filler; O = orientation parameter of the fillers.

This parameter can be used to fit the equation and its value ranges from -1/2 to 1. O = (-) 1/2 corresponds to fillers uniformly oriented normally to the plane of the sample film (orthogonal arrangement) and 1 represents fillers uniformly oriented parallel to the plane of the film. In the case of randomly oriented filler particles, O is equal to zero. Setting O=1 leads to Nielsen's formula, corresponding to particles perpendicularly oriented to the diffusion flux; thus, the model has been applied to predict the dependency of the volume fraction of filler on the permeability of gases. Here, the dependency of orientation and state of dispersion of fillers is not considered. According to this model, the relative permeability of gas molecules as a function of filler volume fraction is given by the following equation.

$$\frac{P}{P_o} = \frac{1-\emptyset_i}{1+\frac{\alpha}{2}\emptyset_i}. \qquad (10)$$

The average values of aspect ratio were deduced from Nielsen's and Bharadwaj model and were estimated to be approximately 179.2 and 222.55, respectively (Fig. 7). The calculated aspect ratio will have disparities because of orientation, entanglement of nanofibers, flexibility and network structure of CNF. Another possible reason for the inconsistent values could be explained by the limitation of theoretical models, which neglect the physical interaction at the filler polymer interface and the chain confinement in
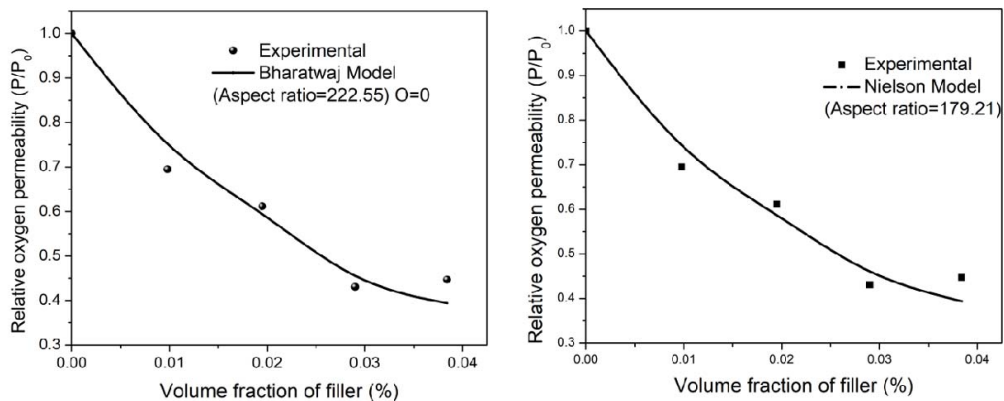

Fig. 7. Experimental values fitted with Bharatwaj and Nielsen models with different weight percentages of CNF

Table 3. Light transmittance of nanocomposites at different wavelengths

Wt.% CNF	Light transmission at different wavelengths (%)						
	200 nm	280 nm	350 nm	400 nm	500 nm	600 nm	700 nm
0	0.42±0.02	30.5±0.01	51.9±1.03	56.1±3.32	60.5±3.27	62.8±1.28	65.5±2.25
1	0.40±0.01	24.6±0.03	43.1±1.36	47.1±4.11	51.2±2.56	53.3±4.68	55.2±3.28
2	0.38±0.01	21.7±0.02	36.5±2.01	39.5±2.65	41.3±1.25	45.3±2.89	47.2±2.69
3	0.32±0.01	18.7±0.04	33.4±1.41	36.7±3.13	40.0±2.14	41.4±3.68	43.9±3.33
4	0.12±0.04	14.3±0.01	27.0±3.64	29.4±2.87	32.2±3.27	33.4±2.11	35.5±3.69

this area (Aulin et al., 2012; Dash and Swain, 2013).

UV-Vis spectroscopy

The packaging was able to absorb light in the UV region to avoid the oxidative rancidity (Castillo et al., 2013; Chen et al., 2013). In case the films were not UV responsive, the packaging films must be irradiated with UV light to destroy the microbial charge (Narayanan et al., 2017). Table 3 shows the transmission values for UV (200-400 nm) and visible (500-700 nm) light. Nanocomposite films have higher transmittance values in the range of visible light compared with ultraviolet light. There is a reduction in the UV absorbance of the nanocomposites after the addition of cellulose nanofibers. This is due to the blocking effect induced by nanoreinforcement; similar findings were also reported by Hietala et al. (2013). This reduction in the light transmittance in the UV region after successive filler incorporations confirms the UV absorption potential of incorporated nanofillers in the matrix. This will certainly help protect food items from UV degradation.

Conclusions

In this study, thermoplastic starch nanocomposites were prepared using a solution casting technique by incorporating cellulose nanofiber from pineapple leaf. Better adhesion and dispersion of cellulose nanomaterials in the starch matrix could lead to better nanocomposite properties compared to the pristine sample. However, at higher filler loading the mechanical and barrier properties were reduced, possibly due to agglomeration. The composites fit well with the Halpin-Tsai model at higher aspect ratios, thereby confirming the long fibrous nature of the filler, which helps to effectively transfer the load. Both water vapor permeability and oxygen permeability decreased with increasing nanofiber content. The tortuosity factor of the nanocomposite increased because of the formation of a more difficult path for the movement of oxygen gas. UV-Vis spectral data confirmed the UV protective properties of the films. The results of the present study could prove that TPS/CNF nanocomposites possess the ability to be used as food packaging materials in the future.

References

Abraham J., Maria H.J., George S.C., Kalarikkal N., Thomas S. (2015) Transport characteristics of organic solvents through carbon nanotube filled styrene butadiene rubber nanocomposites: the influence of rubber–filler interaction, the degree of reinforcement and morphology. *Physical Chemistry Chemical Physics*, 17(17): 11217–11228

Arib R.M.N., Sapuan S.M., Ahmad M.M.H.M., Paridah M.T., Zaman H.M.D.K. (2006) Mechanical properties of pineapple leaf fibre reinforced polypropylene composites. *Materials & Design*, 27(5): 391–396

Aulin C., Salazar-Alvarez G., Lindström T. (2012) High strength, flexible and transparent nanofibrillated cellulose–nanoclay biohybrid films with tunable oxygen and water vapor permeability. *Nanoscale*, 4(20): 6622-6628

Balakrishnan P., Sreekala M.S., Kunaver M., Huskić M., Thomas S. (2017) Morphology, transport characteristics and viscoelastic polymer chain confinement in nanocomposites based on thermoplastic potato starch and cellulose nanofibers from pineapple leaf. *Carbohydrate Polymers*, 169: 176-188

Bertuzzi M.A., Castro Vidaurre E.F., Armada M., Gottifredi J.C. (2007) Water vapor permeability of edible starch based films. *Journal of Food Engineering*, 80(3): 972-978

Biduski B., Silva W.M.F. da, Colussi R., Mello El Halal S.L. de, Lim L.-T., Dias Á.R.G., Zavareze E.R. da (2018) Starch hydrogels: The influence of the amylose content and gelatinization method. *International Journal of Biological Macromolecules*, 113: 443-449

Canisag H. (2015) *Bio-crosslinking of starch films with oxidized sucrose*. Textiles, Merchandising and Fashion Design: Dissertations, Theses, & Student Research, 6

Castillo L., López O., López C., Zaritzky N., García M.A., Barbosa S., Villar M. (2013) Thermoplastic starch films reinforced with talc nanoparticles. *Carbohydrate Polymers*, 95(2): 664–674

Chen H., Zhang W., Du X., Yang J., Zhang N., Huang T., Wang Y. (2013) Crystallization kinetics and melting behaviors of poly (l-lactide)/graphene oxides composites. *Thermochimica Acta*, 566: 57-70

Chivrac F., Angellier-Coussy H., Guillard V., Pollet E., Avérous L. (2010) How does water diffuse in starch/montmorillonite nano-biocomposite materials? *Carbohydrate Polymers*, 82(1): 128–135

Dash S., Swain S.K. (2013) Synthesis of thermal and chemical resistant oxygen barrier starch with reinforcement of nano silicon carbide. *Carbohydrate Polymers*, 97(2): 758–763

Di Y., Kang M., Zhao Y., Yan S., Wang X. (2006) Morphology and mechanical properties of blends of thermoplastic polyurethane and polyolefins. *Journal of Applied Polymer Science*, 99(3): 875–883

Gironès J., López J.P., Mutjé P., Carvalho A.J.F., Curvelo A.A.S., Vilaseca F. (2012) Natural fiber-reinforced thermoplastic starch composites obtained by melt processing. *Composites Science and Technology*, 72(7): 858–863

Grande C.J., Torres F.G., Gomez C.M., Troncoso O.P., Canet-Ferrer J., Martínez-Pastor J. (2009) Development of self-assembled bacterial cellulose–starch nanocomposites. *Materials Science and Engineering: C*, 29(4): 1098–1104

Guohua Z., Ya L., Cuilan F., Min Z., Caiqiong Z., Zongdao C. (2006) Water resistance, mechanical properties and biodegradability of methylated-cornstarch/poly(vinyl alcohol) blend film. *Polymer Degradation and Stability*, 91(4): 703–711

Halley P.J. (2005) Thermoplastic starch biodegradable polymers. *Biodegradable polymers for industrial applications*. Smith R. (ed.) Cambridge, Woodhead Publishing, p. 140-162

Hietala M., Mathew A.P., Oksman K. (2013) Bionanocomposites of thermoplastic starch and cellulose nanofibers manufactured using twin-screw extrusion. *European Polymer Journal*, 49(4): 950–956

Hoyos M., Fina A., Carniato F., Prato M., Monticelli O. (2011) Novel hybrid systems based on poly(propylene-g-maleic anhydride) and Ti-POSS by direct reactive blending. *Polymer Degradation and Stability*, 96(10): 1793–1798

Kraus G. (1963) Swelling of filler-reinforced vulcanizates. *Journal of Applied Polymer Science*, 7(3): 861–871

Malmir S., Montero B., Rico M., Barral L., Bouza R. (2017) Morphology, thermal and barrier properties of biodegradable films of poly (3-hydroxybutyrate-co-3-hydroxyvalerate) containing cellulose nanocrystals. *Composites Part A: Applied Science and Manufacturing*, 93: 41–48

Mlalila N., Hilonga A., Swai H., Devlieghere F., Ragaert P. (2018) Antimicrobial packaging based on starch, poly(3-hydroxybutyrate) and poly(lactic-co-glycolide) materials and application challenges. *Trends in Food Science & Technology*, 74: 1–11

Montaño-Leyva B., Rodriguez-Felix F., Torres-Chávez P., Ramirez-Wong B., López-Cervantes J., Sanchez-Machado D. (2011) Preparation and characterization of durum wheat (Triticum durum) straw cellulose nanofibers by electrospinning. *Journal of Agricultural and Food Chemistry*, 59(3): 870–875

Müller C.M.O., Laurindo J.B., Yamashita F. (2009) Effect of cellulose fibers addition on the mechanical properties and water vapor barrier of starch-based films. *Food Hydrocolloids*, 23(5): 1328–1333

Nair S.B., Alummoottil N.J., Moothandasserry S.S. (2017) Chitosan-konjac glucomannan-cassava starch-nanosilver composite films with moisture resistant and antimicrobial properties for food-packaging applications. *Starch - Stärke*, 69(1-2): 160-210

Narayanan M., Loganathan S., Valapa R.B., Thomas S., Varghese T.O. (2017) UV protective poly(lactic acid)/rosin films for sustainable packaging. *International Journal of Biological Macromolecules*, 99: 37–45

Nielsen L.E. (1967) Models for the permeability of filled polymer systems. *Journal of Macromolecular Science: Part A - Chemistry*, 1: 929–942

Park H.-M., Lee W.-K., Park C.-Y., Cho W.-J., Ha C.-S. (2003) Environmentally friendly polymer hybrids Part I Mechanical, thermal, and barrier properties of thermoplastic starch/clay nanocomposites. *Journal of Materials Science*, 38(5): 909–915

Prachayawarakorn J., Sangnitidej P., Boonpasith P. (2010) Properties of thermoplastic rice starch composites reinforced by cotton fiber or low-density polyethylene. *Carbohydrate Polymers*, 81(2): 425–433

Sadegh-Hassani F., Mohammadi Nafchi A. (2014) Preparation and characterization of bionanocomposite films based on potato starch/halloysite nanoclay. *International Journal of Biological Macromolecules*, 67: 458–462

Tan B., Thomas N.L. (2016) A review of the water barrier properties of polymer/clay and polymer/ graphene nanocomposites. *Journal of Membrane Science*, 514: 595–612

Tang X., Alavi S. (2011) Recent advances in starch, polyvinyl alcohol based polymer blends, nanocomposites and their biodegradability. *Carbohydrate Polymers*, 85(1): 7–16

Wang J., Gardner D.J., Stark N.M., Bousfield D.W., Tajvidi M., Cai Z. (2018) Moisture and oxygen barrier properties of cellulose nanomaterial-based films. *ACS Sustainable Chemistry & Engineering*, 6(1): 49–70

Zeppa C., Gouanvé F., Espuche E. (2009) Effect of a plasticizer on the structure of biodegradable starch/clay nanocomposites: Thermal, water-sorption, and oxygen-barrier properties. *Journal of Applied Polymer Science*, 112(4): 2044–2056